Process modelling, simulation and technoeconomic evaluation of crystallisation antisolvents for the continuous pharmaceutical manufacturing of rufinamide

PROCESS MODELLING, SIMULATION AND TECHNOECONOMIC EVALUATION OF CRYSTALLISATION ANTISOLVENTS FOR THE CONTINUOUS PHARMACEUTICAL MANUFACTURING OF RUFINAMIDE

Samir Diab, Dimitrios I. Gerogiorgis*

Institute for Materials and Processes (IMP), School of Engineering, University of Edinburgh, The King's Buildings, Edinburgh, EH9 3FB, United Kingdom

Corresponding author: D.Gerogiorgis@ed.ac.uk (+44 131 6517072)

Keywords: Continuous pharmaceutical manufacturing (CPM); Rufinamide; Process modelling and simulation; Technoeconomic evaluation; Green chemistry

ABSTRACT

Continuous pharmaceutical manufacturing (CPM) is a promising new paradigm to produce active pharmaceutical ingredients (APIs), allowing reduced equipment dimensions, lower waste production and energy consumption, and safer operation in comparison to the industrially dominant batch methods. Rufinamide is an antiepileptic agent whose demonstrated continuous flow synthesis (featuring three reactions in flow) circumvents the accumulation of toxic and explosive organoazide intermediates. To ascertain the feasibility and viability of this continuous synthetic route, systematic process modelling and costing is required. This paper presents a technoeconomic analysis of the upstream continuous flow synthesis of rufinamide via steady-state process modelling and plantwide simulation. Reaction kinetics and Arrhenius parameters are estimated from previously published experimental data, and plug flow reactor (PFR) volumes are calculated towards rigorous plant costing. Continuous reactor and separator units have been designed, and the CPM flowsheet is compared vs. the batch production method, with respect to technical efficiency and profitability. Plantwide costing via an established economic analysis methodology has been pursued to enable a detailed comparison of cost items towards process scale-up, as well as motivate the need for further systematic optimisation.

1. Introduction

The pharmaceutical industry currently suffers from the highest R&D costs of all manufacturing sectors, significant competition from generics manufacturers, high volumes of waste and narrowing profit margins (Plumb 2005). Improvements in manufacturing methods can allow significant cost savings which could improve the profitability and sustainability of pharmaceutical firms and enterprises (Behr et al. 2004). Technological innovation is required to realise such improvements.

Continuous pharmaceutical manufacturing (CPM) is a new production paradigm recognised by the highest regulatory levels as having the potential to allow significant reductions in environmental impact (Dallinger & Kappe 2017) and cost savings benefits compared to traditionally implemented batch methods (Poechlauer et al. 2013). Despite these benefits, with a number of demonstrated continuous flow syntheses (Britton et al. 2017) and end-to-end campaigns (Mascia et al. 2013; Adamo et al. 2016) for pharmaceutical products in the literature, there is an inertia and stagnancy to the widespread adoption of CPM due to existing investments in established and mature batch technologies (Federsel 2013). Furthermore, issues with continuous downstream processing can present a bottleneck to realising end-to-end CPM campaigns (Rogers & Ierapetritou 2014). Explicit demonstration of the benefits of CPM compared to batch methods is required to facilitate the transition of manufacturing paradigm.

An important advantage of continuous operation is the ability to access process conditions (e.g. high pressure and temperature) that would be otherwise too hazardous to operate in batch mode (Movsisyan et al. 2016); this is due to the improved heat and mass transfer characteristics inherent of the smaller equipment dimensions required for continuous operation compared to batch vessels (Gutmann et al. 2015; Ashe 2012). Operating hazardous reactions is inherently safer in continuous mode due to the limitation of the hazard to a smaller footprint compared to equivalent setups in batch mode.

Active pharmaceutical ingredients (APIs) containing 1,2,3-triazole rings are known to have a wide range of applications including antifungal (Aher et al. 2009), anti-HIV (da Silva et al. 2009), anti-cancer (Kamal et al. 2008), antibacterial (Wang et al. 2010) and tuberculosis treatments (Costa et al. 2006) amongst others. Synthetic routes towards molecules containing 1,2,3-triazole cores require generation of organoazide intermediates which pose significant operational hazards due to their high propensity for detonation (Badgujar et al. 2008). Such reactions in flow can potentially be too hazardous in batch mode due to the accumulation and required isolation of organoazide intermediates between batch unit operations. Continuous operation of such reactions have the potential to circumvent these hazards by generating these intermediates and immediately reacting them in flow (Baumann et al. 2011).

Rufinamide is a societally important API developed for the treatment of Lennox-Gastaut syndrome (Hakimian et al. 2007), present in formulations such as Banzel or Inovelon. Rufinamide contains a 1,2,3-triazole ring whose synthesis requires the generation of organoazide intermediates. Various synthetic routes towards rufinamide have been demonstrated in recent years (Zhang et al. 2014; Mudd & Stevens 2010; Borukhova et al. 2016; Borukhova et al. 2013; Bonacorso et al. 2015) with life cycle assessments also elucidating process benefits of various manufacturing routes (Ott et al. 2016). One of these demonstrations implements a continuous flow synthesis featuring three plug flow reactors (PFRs) whilst avoiding the accumulation or holdup of hazardous organoazide intermediates (Zhang et al. 2014). The continuous flow synthesis is followed by an antisolvent crystallisation implemented in batch mode.

Experimental efforts in elucidating the best process options for CPM application can be costly and time-consuming; process modelling and simulation is a valid method of comparing different options (Teoh et al. 2015) which can establish the most feasible and viable CPM configurations. Various studies in the literature conduct crystallisation kinetic parameter estimation for different crystallisation configurations (Alvarez et al. 2011; Morris et al. 2015; Power et al. 2015; Mitchell et al. 2011; Kwon et al. 2015). Modelling of various conceptual crystallisation processes (Li et al. 2017; Diab & Gerogiorgis 2017b; Sang-Il Kwon et al. 2014) and the development of suitable control schemes for tuning various product characteristics (Su et al. 2015; Su et al. 2017; Nagy et al. 2013) also demonstrate the need for establishing promising candidate configurations prior to expensive experimental investigation. Integrating continuous crystallisation processes into upstream CPM plants is paramount for successful end-to-end implementation.

This work develops a steady-state process model for the simulation of the CPM of rufinamide based on the demonstrated continuous flow synthesis in the literature (Zhang et al. 2014). Reaction kinetic parameter regression, mass balance calculation and reactor sizing are conducted for the upstream CPM of rufinamide. Batch and continuous crystallisation processes following the continuous flow synthetic route are also modelled, implementing API solubility modelling in multicomponent process mixtures to systematically compare different separation options. Subsequent economic analyses elucidates cost savings benefits when implementing continuous crystallisation of the API versus the batch method. A critical discussion of the results, process modelling methodologies and design methods are then provided to examine the technoeconomic feasibility and viability of the CPM of rufinamide.

2. Process Modelling and Simulation

2.1 Process Description and Flowsheet Development

The process model and flowsheet developed here is based on the continuous flow synthesis of rufinamide in a series of plug flow reactors (PFRs) demonstrated by Zhang et al. (2014). The reaction scheme for the CPM of rufinamide is shown in Figure 1 and the developed flowsheet in Figure 2.

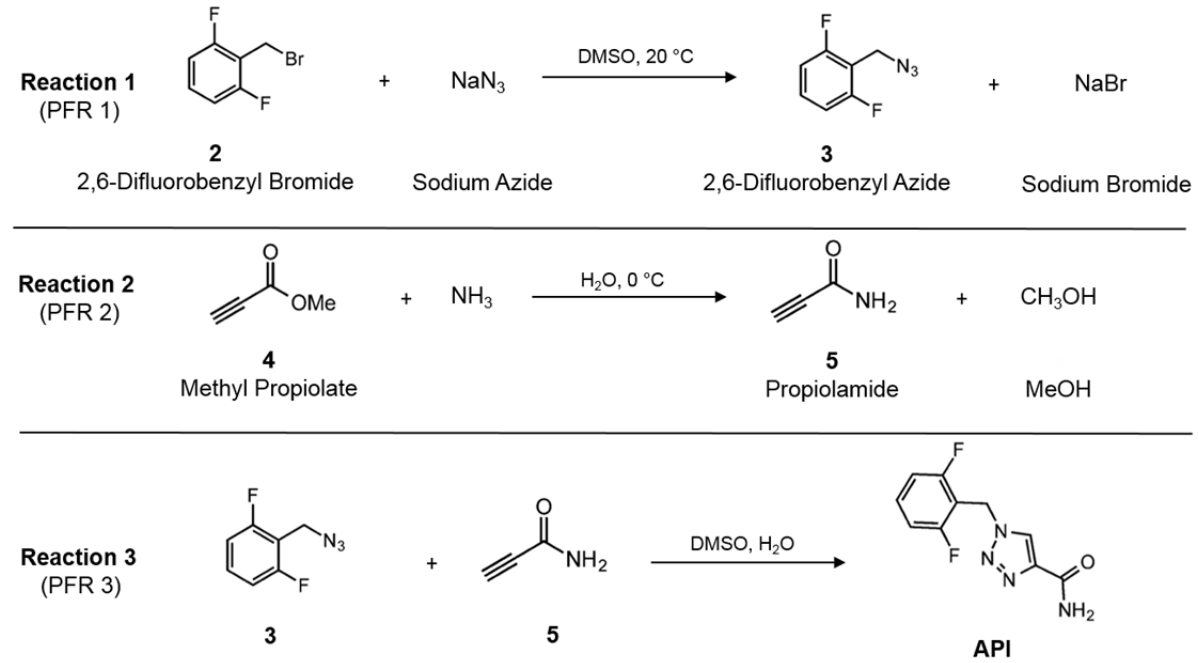

Figure 1: Reaction scheme for the continuous flow synthesis of rufinamide (Zhang et al. 2014).

The first reaction (in PFR-1 in Figure 2) is a S_N2 substitution of 2,6-difluorobenzyl bromide (**2**) by sodium azide (NaN_3) at 20 °C, forming the intermediate 2,6-difluorobenzyl azide (**3**) and sodium bromide (NaBr) as a by-product. Both reagents require dimethyl sulfoxide (DMSO) as a carrier solvent. The second reaction (in PFR-2 in Figure 2) features a mixture of neat methyl propiolate (**4**) and aqueous ammonium hydroxide reacting at 0 °C to form intermediate propiolamide (**5**), condensing methanol (MeOH) as a by-product. Intermediates **3** and **5** mix at a T-junction and enter PFR-3 (Figure 2) to synthesise the API (reaction 3) catalysed by copper reactor tubing (Zhang et al. 2014). The original publication also reports the formation of a regioisomer of rufinamide in PFR-3, which is not considered here due to the lack of available kinetic data for this reaction (Zhang et al. 2014). A back pressure of 100 psi is required to regulate NH_3 gas generation (Zhang et al. 2014). The effluent of PFR-3 (stream F_{17} in Figure 2) then undergoes antisolvent crystallisation (in CR-1 in Figure 2) where rufinamide is crystallised and removed as a solid product (stream F_{19} in Figure 2). The mother liquor containing unreacted reagents, by-products, solvents and antisolvent is removed as waste (stream F_{20} in Figure 2).

Steady-state process modelling and simulation for the CPM of rufinamide assumes a plant capacity of 100 kg API per annum. PFR design requires reaction kinetic parameter regression and mass balance calculations. Process mass balances are calculated based on reported attainable conversion data (Zhang et al. 2014) and are scaled to account for reaction and separation inefficiencies to meet the specified plant capacity. The following general assumptions are made in the process modelling methodology:

1. Reactions occur in the PFRs only and not in any associated connecting lines or units.
2. The only reactions occurring in PFRs-1-3 are those shown in Figure 1.
3. Isothermal operation of all PFRs is ensured by providing suitable heat transfer media and the selection of appropriate PFR dimensions.
4. Temperature changes and reaction/formation of components in the process cause no phase changes or affect the flow, as reported by the authors of the experimental demonstration (Zhang et al. 2014).
5. All process mixtures prior to crystallisation are homogenous and considered ideal solutions.

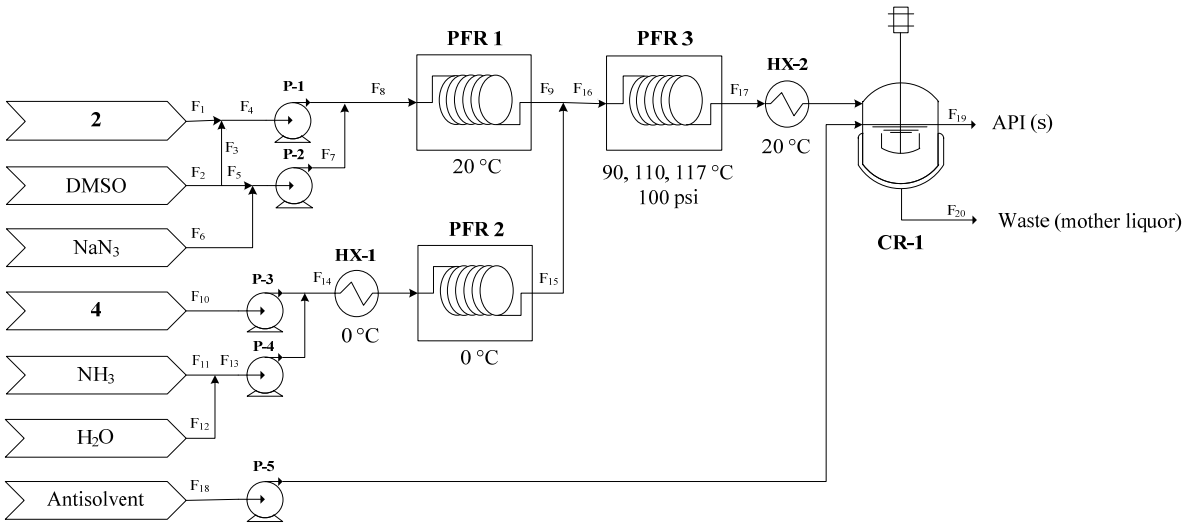

Figure 2: Conceptual flowsheet for continuous upstream production of rufinamide (Zhang et al. 2014).

Molecular weights and densities of process components are required for the conversion of stream flowrates for the purposes of both reactor design, calculation of API mixture solubilities and economic analyses. Physical properties and details of all process components described above for the continuous flow synthesis of rufinamide are listed in Table 1.

Table 1: Process component physical properties

Component	CAS #	MW (g mol^{-1})	ρ (g mL^{-1})	Melting Point (°C)	Boiling Point (°C)
2	85118-00-9	207.02	1.63	53.50	184.90
DMSO	67-68-5	78.13	1.10	19.00	189.00
NaN_3	26628-22-8	65.01	1.85	275.00	300.00
3	106308-60-5	133.15	1.07	unavailable	unavailable
NaBr	7647-15-6	102.89	3.21	747.00	1390.00
4	922-67-8	84.07	0.95	unavailable	104.05
NH_3	7664-41-7	17.03	0.77	-77.73	-33.34
H_2O	7732-18-5	18.02	1.00	0.00	100.00
5	7341-96-0	69.06	1.10	59.50	134.60
MeOH	67-56-1	32.04	0.79	-97.60	64.70
API	106308-44-5	240.21	1.52	198.23	431.97

2.2 Reactor Design

2.2.1 Reaction Kinetic Parameters

Kinetic parameters are required for the design of PFRs. Reaction rate constants are calculated from experimental data and assumptions made are described in this section. The results and assumptions for kinetic parameter estimation are summarised in Tables 2 and 3.

Reactions 1 and 2 (Figure 1) are assumed to be first-order, as they involve large organic molecules (**2** and **4** in Reactions 1 and 2, respectively) reacting with an excess of a smaller molecules (NaN_3 and NH_3 in reactions 1 and 2, respectively). Similar assumptions of first-order reactions between large molecules and excesses of smaller reagents have been made in previous process modelling and simulation efforts (Jolliffe & Gerogiorgis, 2016a); validation of reaction order by comparing candidate rate law expressions for wider kinetic data sets can further validate this assumption. Reaction 3 involves two large organic molecules, for which we compare results considering reaction 3 as either first-order in **3**, or overall second-order (first-order in both **3** and **5**). Here, we describe kinetic parameter estimation methods for all three reactions. Equation 1 is the design equation for a PFR.

$$\tau_j = C_{A,0} \int_0^{X_{f,j}} \frac{dX_A}{-r_A} \tag{1}$$

Here, τ_j is the residence time in PFR j, $C_{A,0}$ is the initial concentration of limiting reagent, $X_{f,j}$ is the final conversion of limiting reagent in PFR j, and r_A is the rate of reaction of the limiting reagent. Expanding and rearranging eq. 1 gives the first- and second-order rate constants in eqs. 2-3, respectively.

$$k_{1,j} = \frac{1}{\tau_j \ln(1 - X_{f,j})} \tag{2}$$

$$k_{2,j} = -\frac{1}{\tau_j C_{A,0}} \int_0^{X_{f,j}} \frac{dX_A}{(1 - X_A)(\Theta_B + \vartheta_B X_A)} \tag{3}$$

$k_{i,j}$ is the i^{th} order rate constant of the reaction occurring in PFR j, Θ_B is the molar ratio of excess reagent to the limiting reagent and ν_B is the stoichiometric coefficient of excess reagent. The integral in eq. 3 is calculated in MS Excel for reported attainable conversions. Eqs. 2-3 allow calculation of reaction rate constants from reported attainable reaction conversions at certain PFR residence times and reagent stoichiometries implemented in the literature (Zhang et al. 2014).

In reaction 1, 1.3 equivalents of NaN_3 react with **2** to form **3**, with a reported conversion of **2** of 100% at room temperature for a residence time of 1 min (Zhang et al. 2014); for modelling purposes, the conversion of **2** has been taken to equal 99.99%. The first-order rate constant of reaction 1 is estimated as $k_{1,1} = 9.21$ min^{-1} using eq. 1 (Table 2).

Reaction 2 involves 4 equivalents of NH_3 reacting with 1 equivalent of **4**; the reported conversion of **4** is 95% at 0 °C for a residence time of 5 min (Zhang et al. 2014). The first-order rate constant of reaction 2 was estimated to be $k_{1,2} = 0.60$ min^{-1} using eq. 1 (Table 2).

Table 2: Kinetic parameter estimation results for reactions in PFRs 1 and 2.

	PFR *j*	
	1	2
Reaction	**2** + NaN_3 → **3**	**4** + NH_3 → **5** + MeOH
Reaction Order, i	1	1
Rate Law	$-r_A = k_{1,1}C_A$	$-r_A = k_{1,2}C_A$
Reactor temperature, T_j (°C)	20	0
Final conversion, X_f (%)	99.99	95
First-order rate constant, $k_{1,j}$ (min^{-1})	9.21	0.60

Figure 3 summarises attainable API yields at varying temperatures for reaction 3 (T_3) reported in for the continuous flow synthesis of rufinamide (Zhang et al. 2014). Attainable API yield decreases beyond a certain temperature due to formation of an API regioisomer. We have fitted a third-order polynomial to the experimental API yield-temperature data, from which the temperature corresponding to the maximum API yield is estimated; this temperature is 117 °C with a maximum API yield of 99.56% (see Figure 3). Below T_3 = 117 °C, it is assumed that only the desired reaction occurs (reaction 3, Figure 1). We calculate first- and second-order rate constants for reaction 3 at temperatures of 90, 110 (considered in the literature) and 117 °C, for which we assume that the only reaction occurring in PFR-3 is reaction 3 (Figure 1).

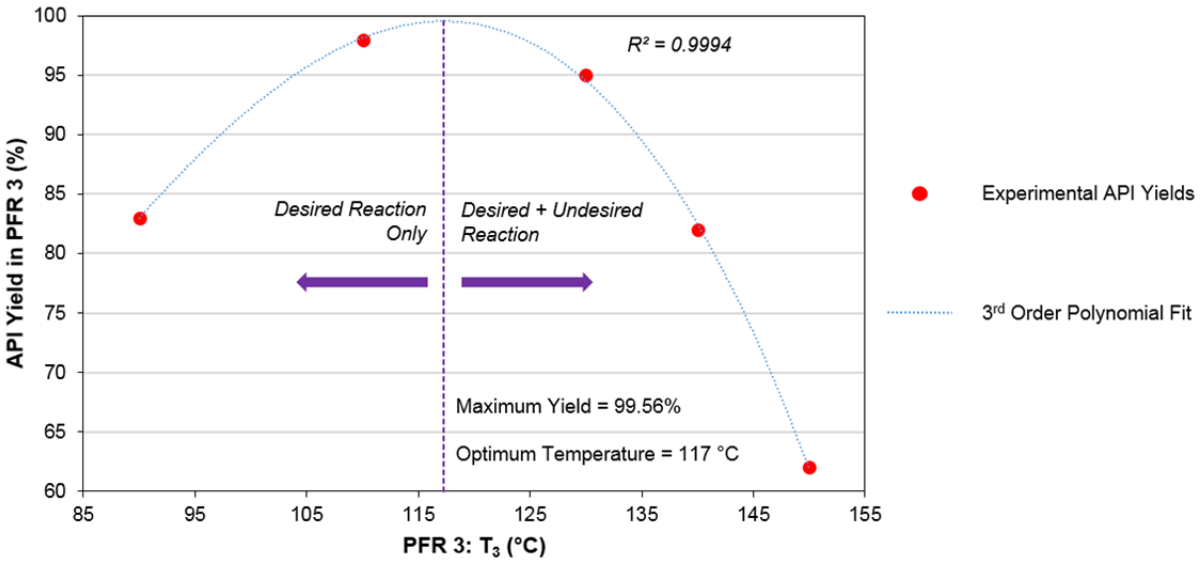

Figure 3: API yield in PFR-3 reported by Zhang et al. (2014) as a function of reaction temperature, T_3.

In reaction 3, 1 equivalent of **3** reacts with 1.42 equivalents of **5** to form rufinamide (API). First- and second-order reaction rate constants were estimated using eqs. 2-3 from attainable conversions of 83%, 98% and 99.56% at operating temperatures (T_3) of 90, 110 and 117 °C, respectively, all for residence times of 6.47 min (Zhang et al. 2014). First- and second-order reaction rate constants for reaction 3 are listed in Table 3.

The Arrhenius law (eq. 4) describes the temperature-dependency of reaction rate constants.

$$k_{i,j}(T_j) = A \exp\left(-\frac{E_a}{RT_j}\right) \tag{4}$$

where A is the pre-exponential factor, E_a is the reaction activation energy and R is the universal gas constant. Values of A and E_a can be estimated from calculated first- and second-order rate constants at different temperatures in PFR-3; these values are provided in Table 3.

Table 3: Reaction kinetics and Arrhenius parameter estimation results for the reaction in PFR 3.

Reaction	**3 + 5 → API**					
PFR 3: T_3 (°C)	90		110		117	
X_A (%)	83		98		99.56	
Reaction Order	1	2	1	2	1	2
Rate Law	$-r_A = k_{1,3}C_A$	$-r_A = k_{2,3}C_AC_B$	$-r_A = k_{1,3}C_A$	$-r_A = k_{2,3}C_AC_B$	$-r_A = k_{1,3}C_A$	$-r_A = k_{2,3}C_AC_B$
$C_{A,0}$ (M)	n.r.	0.248	n.r.	0.248	n.r.	0.248
$k_{i,j}$ (units)	0.27 (min^{-1})	1.34 (M^{-1} min^{-1})	0.60 (min^{-1})	3.51 (M^{-1} min^{-1})	0.79 (min^{-1})	4.85 ($M^{-1}min^{-1}$)

A (—)	$1.06 \cdot 10^6$	$1.28 \cdot 10^8$	$1.06 \cdot 10^6$	$1.28 \cdot 10^8$	$1.06 \cdot 10^6$	$1.28 \cdot 10^8$
E_a (J mol^{-1})	$4.58 \cdot 10^4$	$5.55 \cdot 10^4$	$4.58 \cdot 10^4$	$5.55 \cdot 10^4$	$4.58 \cdot 10^4$	$5.55 \cdot 10^4$

The operating temperature of PFR-3 (T_3) affects the reaction conversion, which alters the process mass balances and total costs of different process designs. We compare the effect of the operating temperature (T_3 = 90, 110 and 117 °C) and the assumed order of reaction 3 (first- and second-order) on process modelling results.

2.2.2 Plug Flow Reactor Design

Reactor volumes are calculated from the required residence time and the material throughput required to attain the specified plant capacity (100 kg API per annum):

$$V_j = \tau_j Q_j \tag{5}$$

where V_i and Q_i are the volume and volumetric flowrate of PFR j, respectively.

2.3 Crystallisation Design

The modelling of crystallisation processes requires API solubility data in multicomponent mixtures. Very limited data for rufinamide solubilities in pure components or mixtures exist in the literature; the experimental solubility of rufinamide in pure DMSO and water at 25 °C (mole fraction solubility = 0.014) is available (Food and Drug Admnistration 2006). Theoretical methods for drug solubility estimation in pure solvents and multicomponent mixtures can be implemented (Bouillot et al. 2011), however essential interaction parameters for even the most established models (UNIFAC, NRTL, NRTL-SAC, COSMO-SAC) are unavailable. A correlation between the octanol-water partition coefficient (ln K_{ow} = -0.12) and the API molar volume (V_m = 212.47 cm^3 mol^{-1}) estimates the API solubility in water (Miller et al. 1985):

$$\ln C_{API}^{sat} = a - bV_m - \ln K_{OW} + \ln F \tag{6}$$

$$\mathrm{F} = \exp\left(\frac{\Delta S}{R}\right)\left(1 - \frac{T_{cryst}}{T_m}\right) \tag{7}$$

$$\frac{\Delta S}{R} \approx 6.8 \tag{8}$$

where C_{API}^{sat} is the solute solubility in water (mol m^{-3}), F is the fugacity ratio, ΔS is the entropy of fusion and T_m is the melting point of the API (see Table 1). a and b are model parameters (a = 3.9 ± 0.2, b = 0.005 ± 0.001). $\Delta S/R$ is taken as 6.8 when data for entropy of fusion is unavailable (Miller et al. 1985). K_{ow} is a function of temperature; a correlation between K_{ow} and temperature is unavailable, so all crystallisation processes are modelled at T_{cryst} = 25 °C.

The API solubility in the mixture is calculated as the sum of mole fraction weighted API solubilities in DMSO (carrier solvent) and water (antisolvent), respectively.

$$S_{API}^{mix} = x_{DMSO}^{mix} S_{API}^{DMSO} + x_{H2O}^{mix} S_{API}^{H2O} \tag{9}$$

where S_{API} is the API mole fraction solubility in a pure solvent or mixture and x_i is the mole fraction of carrier-/antisolvent in the multicomponent mixture. This method allows the comparison of candidate antisolvent crystallisation processes using water as an antisolvent.

The crystallisation yield of API is calculated from the feed API mole fraction and the API mole fraction solubility at saturation

$$Y_i = 100\left(1 - \frac{S_{API}^{mix}}{x_{API}^{feed}}\right) \tag{10}$$

where Y_i is the API crystallisation yield and x_{API}^{feed} is the API mole fraction in the effluent of PFR-3 fed to the crystalliser (CR-1). The method described by eqs. 6-10 was validated by reproducing the experimental batch crystallisation yield of rufinamide within 1%.

In all cases, the effluent of PFR-3 is considered a binary mixture of DMSO and water (single phase) in which all stream components (API, unreacted reagents, byproducts) are considered dissolved solutes. The original continuous flow synthesis publication for rufinamide reports direct batchwise antisolvent crystallisation from the effluent of PFR-3 using water as an antisolvent at an antisolvent-to-feed ratio (AS:F, by mass) of 1.83, with a total crystallisation residence time of 75 min (Zhang et al. 2014). Here, we compare the continuous flow synthesis of rufinamide with the demonstrated batch crystallisation route to that with a conceptual continuous crystallisation method also using water as an antisolvent. For the modelling of continuous crystallisation, we consider antisolvent-to-feed ratios (AS:F, by mass) of 0.25-5 to investigate the effect of varying antisolvent usage. A crystalliser residence time of 60 min is assumed for all CPM processes and a factor of 90% is applied to consider the non-attainment of thermodynamic equilibrium in steady-state (continuous) processes. Crystalliser volumes (V_{cryst}) for CPM processes are calculated from the crystalliser residence time (τ_{cryst}) and the total volumetric flowrate through the crystalliser (Q_{cryst}).

$$V_{cryst} = \tau_{cryst} Q_{cryst} \tag{11}$$

2.4 Environmental Impact Analysis

Ensuring inherently green process designs is essential to ensure low environmental impacts. Recent efforts show significant process improvements in decreasing the quantity of waste produced by a continuous flow synthetic route (Bédard et al. 2016). The environmental impacts of different process options are compared by quantifying green chemistry metrics. Here, we compare the process mass intensities (PMIs) and mass productivities (MPs) of different process options. The PMI quantifies the material input required to produce a unit of material output (Jimenez-Gonzalez et al. 2011):

$$\text{PMI} = \frac{m_{input}}{m_{API}} = \frac{m_{reagents} + m_{solvents} + m_{antisolvents}}{m_{API}} \tag{12}$$

where $m_{reagents}$ is the total mass of reagents required, $m_{solvents}$ is the mass of carrier solvents (DMSO for reaction 1, H_2O for reaction 2), $m_{antisolvent}$ is the mass of antisolvent (H_2O) used for crystallisation and m_{API} is the mass of recovered (crystallised) API. The mass productivity (MP) is another commonly used metric which quantifies how efficiently material is used in a process (Sheldon 2012):

$$\text{MP} = \frac{100}{\text{PMI}} \tag{13}$$

PMIs and MPs are calculated for all batch and CPM processes. For CPM processes, a solvent recovery (carrier and anti-solvents) of 70% is assumed in accordance with previous work (Jolliffe & Gerogiorgis 2016b).

Green chemistry metrics considered here (PMI and MP) are calculated based on the mass of crystalline API obtained only, assuming ideal product purity (100% API). An understanding of impurity component distribution (for which parameters are not available for this specific process) can inform process design for maximum crystal purity (Li et al. 2017). Purification of the effluent of the final PFR prior to continuous crystallisation may be necessary in practice; this may incur additional material requirements that must be included in green chemistry metric calculation. Additional design measures to ensure other desired product attributes, such as crystal size and shape, should also be included and incorporated into comprehensive life-cycle assessment (LCA) studies.

2.5. Economic Analysis

Elucidating cost benefits of CPM over batch technologies is paramount in demonstrating the viability of continuous manufacturing methods (Cervera-Padrell et al. 2012). Our recent work (Jolliffe & Gerogiorgis 2017a; Jolliffe & Gerogiorgis 2017b; Diab & Gerogiorgis 2017a) has implemented a

methodology for the economic analysis of pharmaceutical processes (Schaber et al. 2011). All processes are implemented at an existing pharmaceutical manufacturing site with essential auxiliary infrastructures already in place. 8,040 hours of annual operation are considered in this work.

2.5.1 Capital Expenditure (CapEx)

Prices for equipment of similar capacities to those in this work have been sourced; a cost-capacity correlation is used where equipment of different capacities are found (Woods 2007):

$$C_B = f\, C_A \left(\frac{S_B}{S_A}\right)^n \tag{14}$$

C_j is the equipment purchase cost at capacity S_j. Parameters n and f account for varying design considerations and are found in the literature (Woods 2007). Where the reference purchase cost (C_A) is taken from the past, chemical engineering plant cost indices (CEPCIs) are used to account for inflation. All equipment capacities are scaled to account for PFR and crystalliser inefficiencies to meet the plant capacity. PFRs are priced as microreactors (Corning 2015); solenoid pumps (ProMinent 2015), coolers (Cole-Parmer 2015) and crystalliser (Woods 2007) prices are sourced from historical data. The sum of all inflation-adjusted equipment purchase costs gives the Free-on-Board (FOB) cost. Tables 4 and 5 provide purchase costs and scaling parameters in eq. 14 and the FOB components and total costs for different assumptions of reaction order in PFR-3.

Table 4: Free-On-Board (FOB) costs assuming the reaction in PFR 3 is first-order.

Batch (PFR-3: T_3 = 110 °C)

	Type	Year	CEPCI	f	Basis	n	# Units	C_A (GBP)	S_A	S_B	C_B (GBP)	Total (GBP)
PFR-1	Reactor	2014	578.4	1.0106	V_i (mL)	1.00	1	103,208	80	4.33	5,207	5,207
PFR-2	Reactor	2014	578.4	1.0106	V_i (mL)	1.00	1	103,208	80	3.37	4,055	4,055
PFR-3	Reactor	2014	578.4	1.0106	V_i (mL)	1.00	1	103,208	80	31.63	38,069	38,069
HX-1-2	Cooler	2015	543.0	1.0000	—	1.00	2	3,454	—	—	3,454	6,908
CR-1	Crystalliser	2007	525.4	1.1033	V_{cryst} (m^3)	0.68	1	146,250	75	$1.11 \cdot 10^{-3}$	85	85
P1-5	Pump	2015	543.0	1.0000	—	1.00	5	958	—	—	958	4,790
											FOB (GBP)	59,114

CPM (PFR-3: T_3 = 90 °C)

	Type	Year	CEPCI	f	Basis	n	# Units	C_A (GBP)	S_A	S_B	C_B (GBP)	Total (GBP)
PFR-1	Reactor	2014	578.4	1.0106	V_i (mL)	1.00	1	103,208	80	4.89	5,884	5,884
PFR-2	Reactor	2014	578.4	1.0106	V_i (mL)	1.00	1	103,208	80	3.81	4,582	4,582
PFR-3	Reactor	2014	578.4	1.0106	V_i (mL)	1.00	1	103,208	80	36.28	43,662	43,662
HX-1-2	Cooler	2015	543.0	1.0000	—	1.00	2	3,454	—	—	3,454	6,908
CR-1	Crystalliser	2007	525.4	1.1033	V_{cryst} (m^3)	0.68	1	146,250	75	$1.07 \cdot 10^{-3}$	83	83
P1-5	Pump	2015	543.0	1.0000	—	1.00	5	958	—	—	958	4,790
											FOB (GBP)	65,908

CPM (PFR-3: T_3 = 110 °C)

	Type	Year	CEPCI	f	Basis	n	# Units	C_A (GBP)	S_A	S_B	C_B (GBP)	Total (GBP)
PFR-1	Reactor	2014	578.4	1.0106	V_i (mL)	1.00	1	103,208	80	4.06	4,890	4,890
PFR-2	Reactor	2014	578.4	1.0106	V_i (mL)	1.00	1	103,208	80	3.16	3,807	3,807
PFR-3	Reactor	2014	578.4	1.0106	V_i (mL)	1.00	1	103,208	80	30.15	36,285	36,285
HX-1-2	Cooler	2015	543.0	1.0000	—	1.00	2	3,454	—	—	3,454	6,908
CR-1	Crystalliser	2007	525.4	1.1033	V_{cryst} (m^3)	0.68	1	146,250	75	$8.88 \cdot 10^{-4}$	73	73
P1-5	Pump	2015	543.0	1.0000	—	1.00	5	958	—	—	958	4,790
											FOB (GBP)	56,753

CPM (PFR-3: T_3 = 117 °C)

	Type	Year	CEPCI	f	Basis	n	# Units	C_A (GBP)	S_A	S_B	C_B (GBP)	Total (GBP)
PFR-1	Reactor	2014	578.4	1.0106	V_i (mL)	1.00	1	103,208	80	3.99	4,805	4,805
PFR-2	Reactor	2014	578.4	1.0106	V_i (mL)	1.00	1	103,208	80	3.11	3,742	3,742
PFR-3	Reactor	2014	578.4	1.0106	V_i (mL)	1.00	1	103,208	80	29.63	35,659	35,659
HX-1-2	Cooler	2015	543.0	1.0000	—	1.00	2	3,454	—	—	3,454	6,908
CR-1	Crystalliser	2007	525.4	1.1033	V_{cryst} (m^3)	0.68	1	146,250	75	$8.73 \cdot 10^{-4}$	72	72
P1-5	Pump	2015	543.0	1.0000	—	1.00	5	958	—	—	958	4,790
											FOB (GBP)	55,976

The Chilton method is used to calculated the Battery Limits Installed Cost (BLIC)(Couper 2003). The installed equipment cost (IEC) is 1.43 times the FOB. Process piping and instrumentation (PPI) costs are 42% of IEC, respectively. The sum of IEC and PPI gives the total physical plant cost (TPPC). A construction factor of 0.3 is added to the TPPC to calculate the BLIC.

$$\mathrm{IEC} = 1.43\mathrm{FOB} \tag{15}$$

$$\mathrm{PPI} = 0.42\mathrm{IEC} \tag{16}$$

$$\mathrm{TPPC} = \mathrm{IEC} + \mathrm{PPI} \tag{17}$$

$$\mathrm{BLIC} = 1.3\mathrm{TPPC} \tag{18}$$

Working capital costs are taken as 35% and 3.5% of annual material costs ($\mathrm{MAT_{annual}}$, assuming 70% solvent recovery for CPM processes) for batch and CPM processes, respectively. Annual material costs for batch processes have an added factor of 60% to account for labour and handling (Schaber et al. 2011). Contingency costs (CC) are calculated as 20% of the BLIC. The sum of working capital and contingency costs (WCC) and BLIC gives the total capital expenditure (CapEx) of the process.

$$\mathrm{WC} = \begin{cases} 0.350\mathrm{MAT_{annual}}\text{ , batch} \\ 0.035\mathrm{MAT_{annual}}\text{ , CPM} \end{cases} \tag{19}$$

$$\mathrm{CC} = 0.2\mathrm{BLIC} \tag{20}$$

$$\mathrm{WCC} = \mathrm{WC} + \mathrm{CC} \tag{21}$$

$$\mathrm{CapEx} = \mathrm{BLIC} + \mathrm{WCC} \tag{22}$$

Table 5: Free-On-Board (FOB) costs assuming the reaction in PFR 3 is second-order.

Batch (PFR-3: T_3 = 110 °C)

	Type	Year	CEPCI	f	Basis	n	# Units	C_A (GBP)	S_A	S_B	C_B (GBP)	Total (GBP)
PFR-1	Reactor	2014	578.4	1.0106	V_i (mL)	1.00	1	103,208	80	4.33	5,207	5,207
PFR-2	Reactor	2014	578.4	1.0106	V_i (mL)	1.00	1	103,208	80	3.37	4,055	4,055
PFR-3	Reactor	2014	578.4	1.0106	V_i (mL)	1.00	1	103,208	80	33.84	40,721	40,721
HX-1-2	Cooler	2015	543.0	1.0000	—	1.00	2	3,454	—	-	3,454	6,908
CR-1	Crystalliser	2007	525.4	1.1033	V_{cryst} (m^3)	0.68	1	146,250	75	$1.11 \cdot 10^{-3}$	85	85
P1-5	Pump	2015	543.0	1.0000	—	1.00	5	958	—	-	958	4,790
											FOB (GBP)	61,766

CPM (PFR-3: T_3 = 90 °C)

	Type	Year	CEPCI	f	Basis	n	# Units	C_A (GBP)	S_A	S_B	C_B (GBP)	Total (GBP)
PFR-1	Reactor	2014	578.4	1.0106	V_i (mL)	1.00	1	103,208	80	4.89	5,884	5,884
PFR-2	Reactor	2014	578.4	1.0106	V_i (mL)	1.00	1	103,208	80	3.81	4,582	4,582
PFR-3	Reactor	2014	578.4	1.0106	V_i (mL)	1.00	1	103,208	80	38.80	46,699	46,699
HX-1-2	Cooler	2015	543.0	1.0000	—	1.00	2	3,454	—		3,454	6,908
CR-1	Crystalliser	2007	525.4	1.1033	V_{cryst} (m^3)	0.68	1	146,250	75	$1.07 \cdot 10^{-3}$	83	83
P1-5	Pump	2015	543.0	1.0000	—	1.00	5	958	—		958	4,790
											FOB (GBP)	68,946

CPM (PFR-3: T_3 = 110 °C)

	Type	Year	CEPCI	f	Basis	n	# Units	C_A (GBP)	S_A	S_B	C_B (GBP)	Total (GBP)
PFR-1	Reactor	2014	578.4	1.0106	V_i (mL)	1.00	1	103,208	80	4.06	4,890	4,890
PFR-2	Reactor	2014	578.4	1.0106	V_i (mL)	1.00	1	103,208	80	3.16	3,807	3,807
PFR-3	Reactor	2014	578.4	1.0106	V_i (mL)	1.00	1	103,208	80	32.25	38,812	38,812
HX-1-2	Cooler	2015	543.0	1.0000	—	1.00	2	3,454	—		3,454	6,908
CR-1	Crystalliser	2007	525.4	1.1033	V_{cryst} (m^3)	0.68	1	146,250	75	$8.88 \cdot 10^{-4}$	73	73
P1-5	Pump	2015	543.0	1.0000	—	1.00	5	958	—		958	4,790
											FOB (GBP)	59,280

CPM (PFR-3: T_3 = 117 °C)

	Type	Year	CEPCI	f	Basis	n	# Units	C_A (GBP)	S_A	S_B	C_B (GBP)	Total (GBP)
PFR-1	Reactor	2014	578.4	1.0106	V_i (mL)	1.00	1	103,208	80	3.99	4,805	4,805

PFR-2	Reactor	2014	578.4	1.0106	V_i (mL)	1.00	1	103,208	80	3.11	3,742	3,742
PFR-3	Reactor	2014	578.4	1.0106	V_i (mL)	1.00	1	103,208	80	31.69	38,142	38,142
HX-1-2	Cooler	2015	543.0	1.0000	—	1.00	2	3,454	—		3,454	6,908
CR-1	Crystalliser	2007	525.4	1.1033	V_{cryst} (m^3)	0.68	1	146,250	75	$8.73 \cdot 10^{-4}$	72	72
P1-5	Pump	2015	543.0	1.0000	—	1.00	5	958	—		958	4,790
											FOB (GBP)	58,459

2.5.2 Operating Expenditure (OpEx)

Material purchase prices are sourced from various vendors (Table 6). All material requirements are scaled to account for plantwide inefficiencies to meet the specified plant capacity (100 kg per annum) and provided in Table 6. Annual utilities costs ($UTIL_{annual}$) are calculated as 0.96 GBP kg^{-1} of material. Annual waste costs ($Waste_{annual}$) are 0.35 GBP L^{-1} of waste carrier- and anti-solvent.

$$UTIL_{annual} = 0.96 MAT_{annual} \tag{23}$$

$$Waste_{annual} = 0.35 \left(\frac{m_{20}^{DMSO}}{\rho_{DMSO}} + \frac{m_{20}^{H2O}}{\rho_{H2O}} \right) (1 - SR) \tag{24}$$

$$U\&W_{annual} = UTIL_{annual} + Waste_{annual} \tag{25}$$

where m_{20}^{DMSO} and m_{20}^{H2O} are the mass flowrates of DMSO and water in waste stream F_{20}, respectively (Figure 2), and SR is the solvent recovery (70% for CPM processes).

Table 6: Material requirements of the process with batch and CPM crystallisation methods for varying design assumptions (operating temperature of PFR-3, T_3).

	Batch (kg y^{-1})		CPM (kg y^{-1})		Price (GBP kg^{-1})
T_3 (°C)	110	90	110	117	
2	115	130	108	106	2,560.00
DMSO	2,137	724	602	592	2.31
NaN_3	45	51	42	42	541.00
4	70	79	66	64	4,649.00
NH_3	57	64	53	64	0.19
H_2O	4,985	1,846	1,534	1,507	0.60
Total	**7,409**	**2,893**	**2,405**	**2,375**	

2.5.3 Total Costs

Total material (MAT_{total}) and utilities and waste ($U\&W_{total}$) costs are calculated as the inflation-adjusted annual material and U&W costs, respectively. Total operating expenditure ($OpEx_{total}$) is taken as the sum of total material and U&W.

$$MAT_{total} = \sum_{k=1}^{\tau} \frac{MAT_{annual}}{(1+r)^k} \tag{26}$$

$$U\&W_{total} = \sum_{k=1}^{\tau} \frac{U\&W_{annual}}{(1+r)^k} \tag{27}$$

$$OpEx_{total} = MAT_{total} + U\&W_{total} \tag{28}$$

A total plant-operating lifetime (τ) of 20 years and an interest rate (r) of 5% are considered. The total cost of the plant designs is calculated as the sum of CapEx and inflation-adjusted OpEx over the plant lifetime.

$$\text{Total Costs} = CapEx + OpEx_{total} \tag{29}$$

All CapEx is assumed to occur in year 0 and operation is assumed to begin in year 1.

3. Results and Discussion

3.1 Mass Balances

The calculated mass balances are based on the process for the continuous flow synthesis of rufinamide (API) described by Zhang et al. (2014). Component mass flowrates of key flowsheet streams (Figure 2) for all considered operating temperatures of PFR-3 (T_3 = 90, 110 and 117 °C) are shown in Figure 4; these streams are the feed to PFR-1 (F_8), PFR-2 (F_{14}) and PFR-3 (F_{16}) and the effluent of PFR-3 (F_{17}) prior to crystallisation. All streams have been scaled to account for reaction and crystallisation inefficiencies to the meet the specified plant capacity (100 kg API per annum).

For all CPM process variations (different considerations of the operating temperature of PFR-3), DMSO (the carrier solvent in PFR-1) contributes a significant portion of the total mass balance throughout the whole process. Reagents for reaction 1 in PFR-1 (**2** and NaN_3) are nearly negligible in streams following PFR-1 (F_{16} and F_{17} in Figure 2) due to the high attainable conversion (99.99% assumed here). Similarly, the reagents for reaction 2 and PFR-2 (**4** and NH_3) are in trace quantities following PFR-2 due to the high conversion attained in the reactor. Due to these high conversions, there are significant quantities of desired intermediates (**3** and propiolamide) and by-products (NaBr and MeOH) in the feed to PFR-3 (F_{16} in Figure 2). Rufinamide (API) is present in significant quantities due to the high conversions attained at all PFR-3 operating temperatures (T_3) considered and to account for subsequent crystallisation inefficiencies.

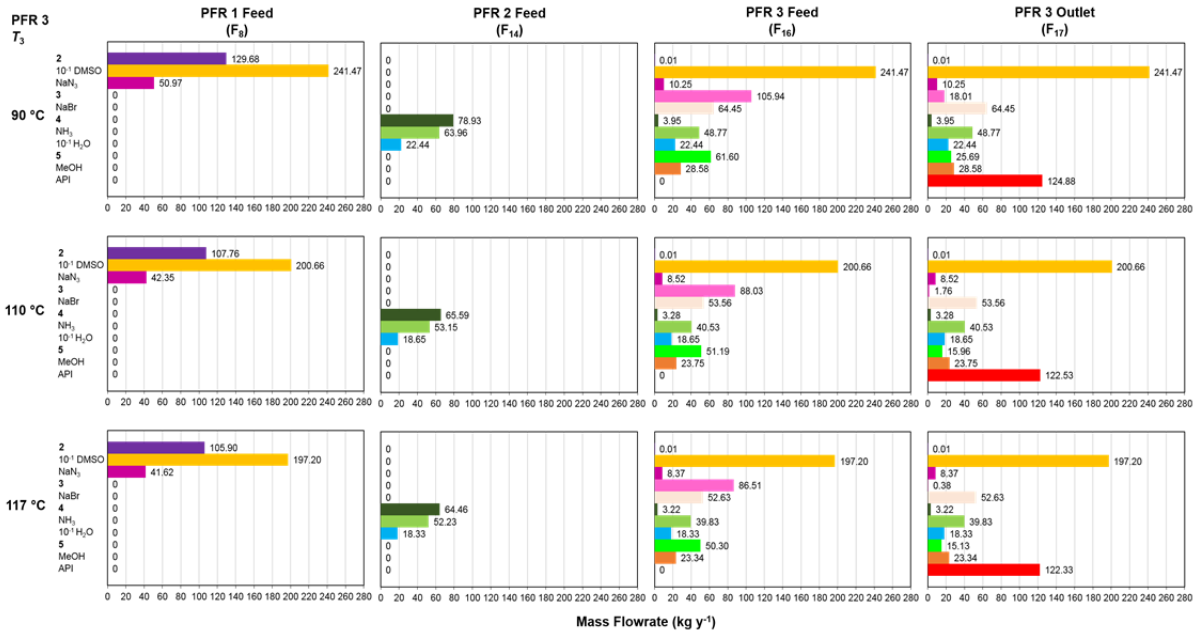

Figure 4: Process mass balances of key flowsheet streams for the CPM of rufinamide under different considerations of the operating temperature of PFR 3 (T_3).

3.2 Plug Flow Reactor Design

PFR volumes are calculated (Figure 5) from required reaction residence times to meet reported attainable conversions and material throughputs calculated from process mass balances. Small reactor volumes are calculated for PFRs-1 and 2 for all PFR-3 operating temperatures (T_3) considered; this is due to the high attainable conversions (99.99% and 95% in PFRs-1 and 2, respectively) short residence times (1 and 5 min for PFRs-1 and 2, respectively) and low material throughputs required to meet the desired plant capacity. Computed volumes for PFR-3 for all considered operating temperatures (T_3) and both reaction order assumptions are higher due to the higher material throughput and longer residence time (6.47 min) required to reach the target attainable conversions compared to the previous PFRs.

Appropriate choice of the internal diameter of PFRs (d_i) is an important design parameter for the resulting reactor length as well as ensuring negligible axial temperature and concentration gradients

(Roberge et al. 2005). Here, we consider PFR inner diameters of 2.5–15.0 mm, in accordance with reported microreactor applications (Wilms et al. 2009; Mascia et al. 2013). Resulting reactor lengths for different inner diameters are shown in Figure 6 for all PFR-3 design variations. Reactor lengths vary from very small (< 10 cm) to considerable sizes (< 750 cm). Reactors of significant length can be coiled in order to reduce the overall equipment size and maintain the benefit of small plant footprint available via continuous operation (Mascia et al. 2013; Ashe 2012; Kopetzki et al. 2013).

Figures 5 and 6 show only a small difference in PFR volumes and lengths between different considerations of first- and second-order assumptions for reaction 3. It is important to note that these results neglect the undesired side reaction forming a regioisomer of rufinamide in PFR-3, which will affect the results presented here. It has been assumed that only the desired reaction occurs in PFR-3 for the operating temperatures considered in this work. Kinetic data for this side reaction is required to estimate accurate reactor volumes and dimensions.

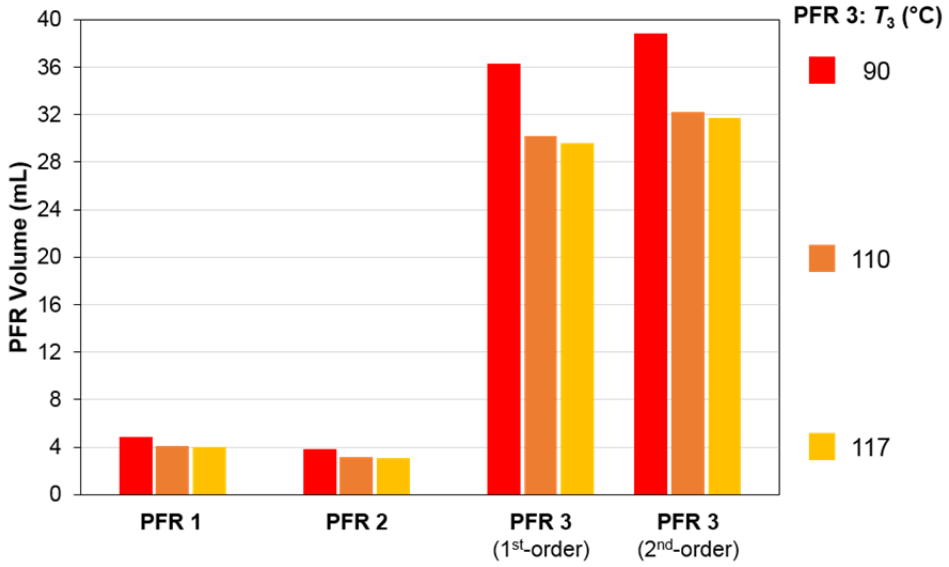

Figure 5: PFR volumes for different assumptions of temperature and reaction order in PFR-3.

3.3 Crystallisation Design

Calculated API mixture solubilities and attainable crystallisation yields for continuous crystallisation of rufinamide from the effluent of PFR-3 (F_{17} in Figure 2) using water as an antisolvent are shown in Figure 7. Antisolvent-to-feed ratios (AS:F, by mass) of 0.25-5 are considered for continuous crystallisation from the effluents of PFR-3 for all operating temperatures of PFR-3 considered. In all cases, increasing AS:F decreases the API mixture solubility and thus increases the attainable crystallisation yield. Non-attainment of thermodynamic (solid-liquid) equilibrium when operating in continuous crystallisation mode is accounted for by applying a factor of 90% to all attainable yields.

Beyond AS:F = 2, the crystallisation yield only increases incrementally, and thus the increased antisolvent usage and resulting crystalliser volumes will lead to unnecessary increases in CapEx, OpEx and PMIs (implying greater quantities of waste to treat). For this reason, continuous crystallisation processes using AS:F = 2 is chosen for all subsequent economic analyses.

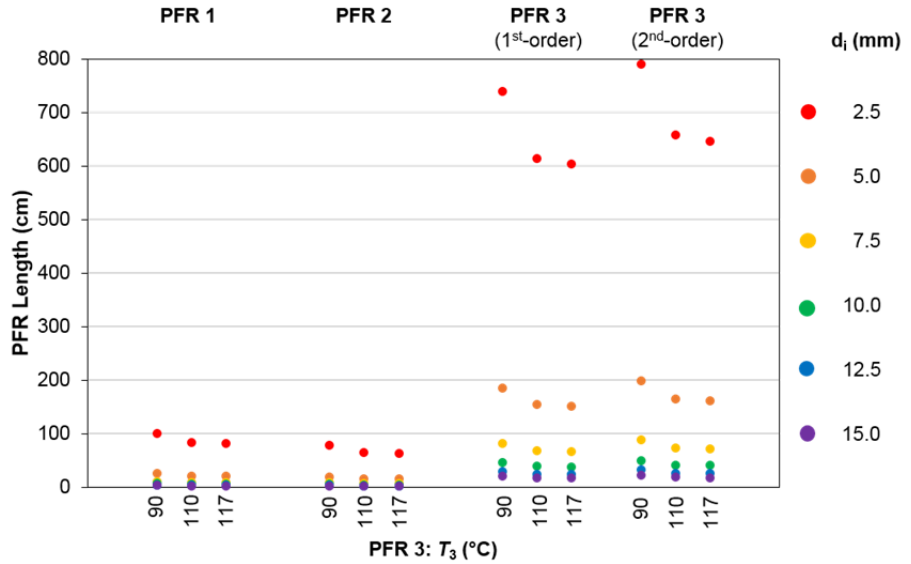

Figure 6: PFR lengths for varying inner diameters (d_i) for different assumptions of the temperature and reaction order in PFR 3.

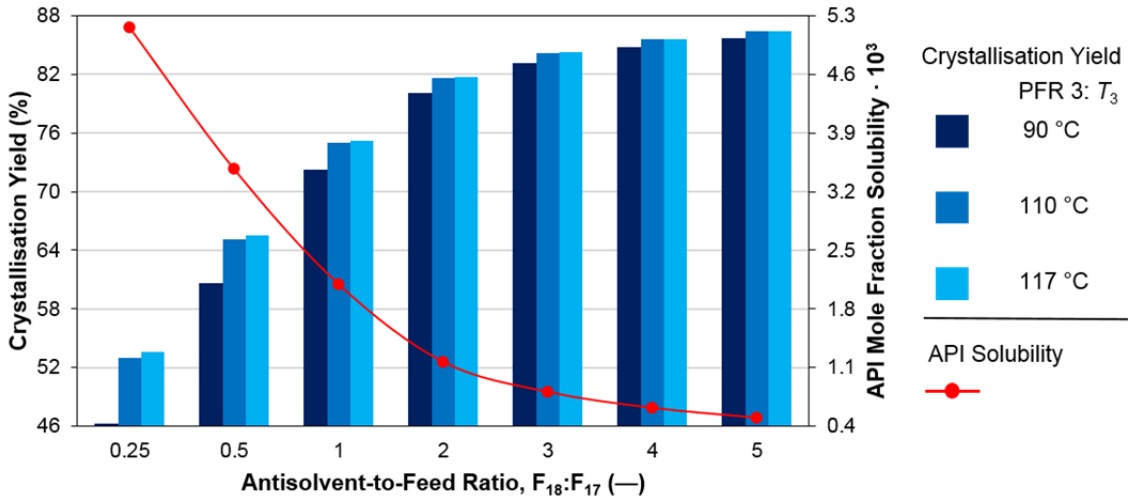

Figure 7: API mixture solubility and attainable crystallisation yield as a function of antisolvent usage and operating temperature of PFR-3 (T_3).

3.4 Environmental Impact Analysis

Process mass intensities (PMIs) and mass productivities (MPs) for the batch process and varying CPM process considerations (different PFR-3 operating temperatures, T_3) are shown in Figure 8. CPM process options consider 70% recovery of carrier- and anti-solvent following continuous crystallisation; AS:F = 1.83 for batch crystallisation (Zhang et al. 2014) and AS:F = 2 for all continuous crystallisations. As the operating temperature in PFR-3 (T_3) increases, PMIs decrease and, correspondingly, MPs increase due to the increased plantwide API recoveries attainable as the conversion in PFR-3 increases. PMIs of typical pharmaceutical processes can be as high as 200 due to the inherent complexity of required manufacturing stages involving multistep syntheses, intermediate workups and purifications etc. (Ritter 2013). These results show the significant improvements in material efficiency and reduction in environmental impact available via CPM implementation from the improved green chemistry metrics compared to the batch process, as shown in Figure 8.

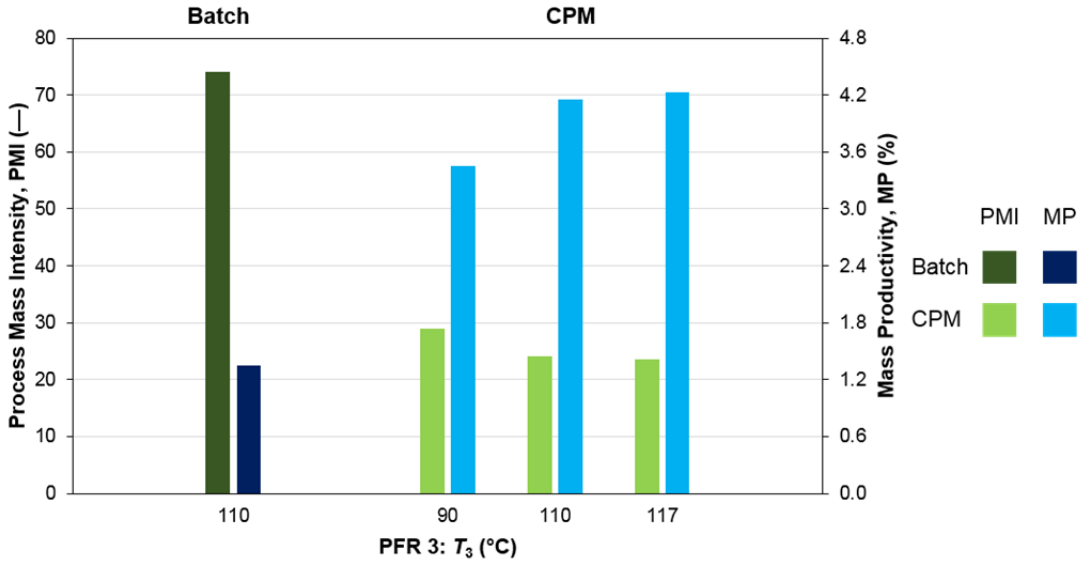

Figure 8: Process mass intensities (PMIs) and mass productivities (MPs) of the process with batch and continuous crystallisation options for different assumptions of the operating temperature of PFR 3 (T_3).

3.5 Economic Analysis

Unit capacities and material requirements are scaled to account for reaction and crystallisation inefficiencies to meet the specified plant capacity (100 kg API per annum). A comparison between different total cost components between processes with a batch crystallisation process and a continuous crystallisation from the effluent of PFR-3, considering different operating temperatures of PFR-3 (T_3). The batch crystallisation process uses AS:F = 1.83 and all continuous crystallisations use AS:F = 2 with an assumed 70% recovery of carrier- and antisolvents. Table 7 shows the calculated cost components and differences between batch and CPM process variations.

Table 7: Cost components (10^3 GBP) and differences between batch and CPM processes for different operating temperatures in PFR 3 (T_3).

PFR 3 = 1st order

	Batch	CPM (AS:F = 2; SR = 70%)					
T_3 (°C)	110	90		110		117	
	Cost	Cost	Difference	Cost	Difference	Cost	Difference
BLIC	156	174	+11.5%	150	–4.0%	148	–5.3%
WCC	396	60	–84.8%	51	–87.1%	50	–87.3%
CapEx	552	234	–57.5%	201	–63.6%	198	–64.1%
10^{-1} · Materials	1,298	909	–30.0%	909	–30.0%	909	–30.0%
10^{-1} · U&W	1,249	874	–30.1%	874	–30.1%	874	–30.1%
10^{-1} · OpEx	2,547	1,783	–30.0%	1,783	–30.0%	1,783	–30.0%
Total	26,020	18,060	–30.6%	18,027	–30.7%	18,024	–30.7%

PFR 3 = 2nd order

	Batch	CPM (AS:F = 2; SR = 70%)					
T_3 (°C)	110	90		110		117	
	Cost	Cost	Difference	Cost	Difference	Cost	Difference
BLIC	163	182	+16.6%	156	+0.3%	154	–1.1%
WCC	397	62	–84.4%	53	–86.7%	52	–86.9%
CapEx	560	244	–55.8%	209	–62.1%	206	–62.7%
10^{-1} · Materials	1,298	909	–30.0%	909	–30.0%	909	–30.0%
10^{-1} · U&W	1,249	874	–30.1%	874	–30.1%	874	–30.1%
10^{-1} · OpEx	2,547	1,783	–30.0%	1,783	–30.0%	1,783	–30.0%
Total	26,028	18,069	–30.6%	18,035	–30.7%	18,032	–30.7%

BLIC savings are only attainable for T_3 = 110 and 117 °C when a first-order reaction in PFR-3 is considered, and only for T_3 = 117 °C when a second-order reaction in PFR-3 is considered. This is due to the higher plantwide API recoveries attainable when implementing a batch crystallisation compared to the continuous crystallisation when PFR-3 is operated at lower temperatures; lower recoveries require increased material throughputs to meet the plant capacity and thus larger equipment. WCC costs are significantly lower for all continuous options considered due to the significantly lower solvent requirements due to the solvent recovery option considered for CPM as well as the additional labour and handling requirements of the batch process. Correspondingly, both material and U&W costs are significantly lower for all CPM options compared to the process implementing batch crystallisation.

CapEx, OpEx and total cost savings of CPM options relative to the process implementing batch crystallisation for varying PFR-3 design assumptions are shown in Figure 9. It is shown that varying the operating temperature in PFR-3 (T_3) and different assumptions of reaction order (first- or second-order) have little effect on the calculated total cost components. CapEx savings variations across different design options are observed due to the effect of PFR-3 operating temperature (T_3) on conversion, and thus plantwide API yield, which directly affects the required material throughput and unit sizes. OpEx costs show little variation for each PFR-3 operating temperature (T_3) chosen for first- and second-order reaction assumptions (in PFR-3) due to similar mass balances and identical solvent recoveries (70%). Thus, there is little variation in total cost savings for different design assumptions for PFR-3. This shows that the reaction order in PFR-3 has only a slight effect on the CPM process. Nevertheless, it is imperative to make informed decisions from detailed kinetic data to present accurate cost components for different process options.

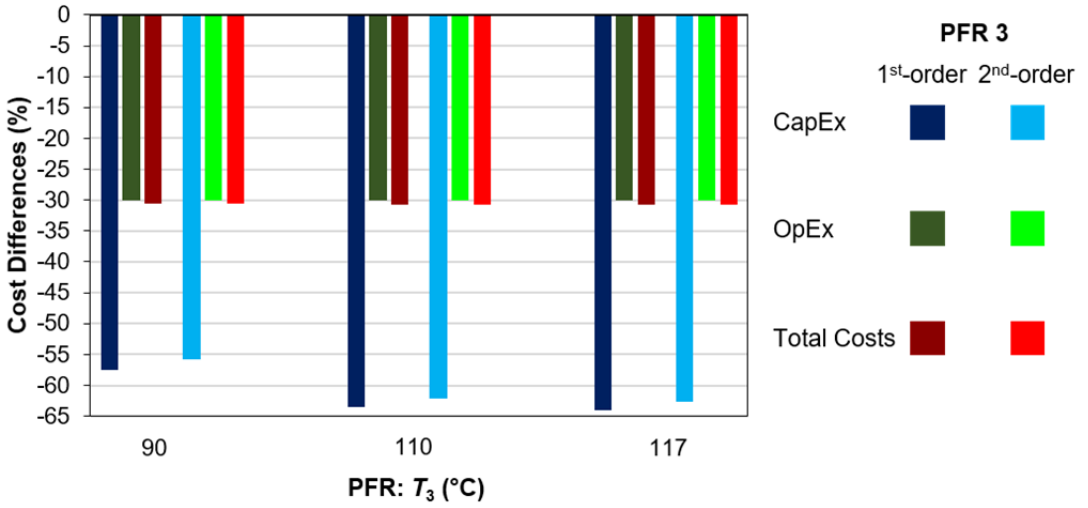

Figure 9: Cost savings of implementing a continuous crystallisation process relative to implementing a batchwise crystallisation.

4. Conclusions

Rufinamide is a societally important API that requires materially efficient and economically viable manufacturing methods. This work has developed a steady-state process model for the CPM of rufinamide for a plant capacity of 100 kg per annum. The model is based upon a published continuous flow synthetic route featuring three plug flow reactors for the synthesis of the API (Zhang et al. 2014) which circumvents the accumulation or isolation of hazardous intermediate organoazides required for the generation of molecules containing 1,2,3-triazole rings. The demonstrated route features short residence times and high conversions towards rufinamide.

The technoeconomic evaluation conducted in this work features kinetic parameter estimation for different assumptions of the reaction order in the final PFR, reactor sizing based on mass balance

calculations and the desired API plant capacity for different operating temperatures of the final PFR, comparison of batch and continuous crystallisation routes via API solubility modelling in multicomponent mixtures (Miller et al. 1985) and economic analyses to establish cost savings attainable when implementing a continuous crystallisation with respect to the batch crystallisation. The process modelling and technoeconomic evaluation follow published methodologies for a new API for which process modelling has not been previously conducted.

Small PFR volumes and lengths for the specified plant capacity are computed for all process design variations (different assumptions on the reaction order in the final PFR and its operating temperature), demonstrating a clear CPM advantage. Calculated crystallisation yields for varying extents of antisolvent usage account for non-attainment of thermodynamic equilibria typical of steady-state (continuous) operation. Environmental impacts of different process options are compared via two popular green chemistry metrics (the process mass intensity, PMI, and the mass productivity, MP) which quantify the material efficiency of manufacturing processes; results show a significant reduction in environmental impact when implementing a continuous crystallisation method compared to the batch crystallisation (lower PMIs and higher MPs). Cost estimations follow an established methodology for batch and continuous pharmaceutical processes (Schaber et al. 2011) and show significant total cost savings when implementing a continuous crystallisation process with respect to the batch crystallisation route. Various assumptions in our process modelling methodology affect these results (e.g. extent of solvent recovery, various costing considerations etc.) but they have been documented in this work to allow reproducibility and to allow future sensitivity analyses of various design parameters.

The process modelling and simulation for the CPM of rufinamide demonstrated in this work shows the importance of conducting such conceptual studies for pharmaceutical processes prior to further development and scale-up. The results demonstrate the environmental and economic benefits of continuous operation for the manufacturing of this societally important API. The potential for a scaled-up application of this process must be further developed by considering its implementation when integrated with subsequent essential downstream unit operations. Subsequent technoeconomic optimisation via non-linear programming with detailed experimental data (including kinetics for side reactions described in the continuous flow synthesis experimental publication) can elucidate the best operating parameters and process configurations for CPM implementation.

5. Acknowledgements

The authors gratefully acknowledge the financial support of the Engineering and Physical Sciences Research Council (EPSRC) via a Doctoral Training Partnership (DTP) PhD fellowship awarded to Mr. Samir Diab (Grant # EP/N509644/1).

6. Nomenclature and Acronyms

Latin Letters and Acronyms

a	Parameter in eq. 6
A	Pre-exponential factor in Arrhenius law (–)
API	Active pharmaceutical ingredient
AS:F	Antisolvent-to-feed ratio by mass (F_{18}:F_{17} in Figure 2)
b	Parameter in eq. 6
BLIC	Battery limits installed costs (GBP)
C_A	Concentration of limiting reagent (M)
$C_{A,0}$	Initial concentration of limiting reagent (M)
C_{API}^{sat}	API saturation concentration in water (mol m^{-3})
C_i	Purchase cost of equipment at capacity i (GBP)
CapEx	Capital expenditure (GBP)
CC	Contingency costs (GBP)
CEPCI	Chemical engineering plant cost index
CPM	Continuous pharmaceutical manufacturing
d_i	PFR inner diameter (mm)
DMSO	Dimethyl sulfoxide

E_a	Activation energy of reaction *j* (J mol^{-1})
F	Fugacity ratio (–)
f	Correction factor in eq. 14
FOB	Free-on-board costs (GBP)
IEC	Installed equipment costs (GBP)
$k_{i,j}$	i^{th} order rate constant of the reaction in PFR *j* (min^{-1} or M^{-1}min^{-1})
K_{OW}	API octanol-water partition coefficient (–)
LCA	Life-cycle assessment
m_j^i	Mass flowrate of component *i* in stream *j* in Figure 2 (kg y^{-1})
$m_{antisolvent}$	Mass of antisolvent fed to the process (kg y^{-1})
m_{API}	Mass of API produced (kg y^{-1})
m_{input}	Mass of material input through the process (kg y^{-1})
$m_{reagents}$	Mass of reagents fed to the process (kg y^{-1})
$m_{solvent}$	Mass of carrier solvent fed to the process (kg y^{-1})
MAT_{annual}	Annual material costs (GBP y^{-1})
MAT_{total}	Total material costs over the plant lifetime (GBP)
MeOH	Methanol
MP	Mass productivity (%)
MW	Molecular weight (g mol^{-1})
n	Exponent in eq. 14
$OpEx_{total}$	Total operating expenditure over the plant lifetime (GBP)
PFR	Plug flow reactor
PMI	Process mass intensity (–)
PPI	Process piping and instrumentation costs (GBP)
Q_{cryst}	Volumetric flowrate through the crystalliser (mL min^{-1})
Q_j	Volumetric flowrate through PFR *j* (mL min^{-1})
R	Universal gas constant (= 8.314 J mol^{-1} K^{-1})
r	Interest rate (%)
r_A	Rate of reaction of limiting reagent (M min^{-1})
S_{API}^{j}	API mole fraction solubility in solvent *j* (–)
S_j	Capacity of equipment (varying units)
ΔS	Entropy of fusion (J mol^{-1} K^{-1})
SR	Solvent recovery (%)
T_{cryst}	Crystallisation temperature (25 °C)
T_j	Operating temperature of PFR *j*
T_m	API melting point (°C)
TPPC	Total physical plant cost (GBP)
$U\&W_{annual}$	Sum of annual annual utilities and waste disposal costs (GBP y^{-1})
$U\&W_{total}$	Total utilities and waste disposal costs over the plant lifetime (GBP)
$UTIL_{annual}$	Annual utilities costs (GBP y^{-1})
V_j	Volume of PFR *j* (mL)
V_{cryst}	Crystalliser volume (mL)
V_m	API molar volume (cm^3 mol^{-1})
WC	Working capital costs (GBP)
WCC	Working capital and contingency costs (GBP)
X_A	Conversion of limiting reagent (%)
X_f	Final attainable conversion of limiting reagent (%)
x_i	Mole fraction of component *i* (–)
Y_i	Crystallisation yield (%)

Greek letters

Θ_B	Mole ratio of excess reagent to limiting reagent (–)
ν_B	Stoichiometric coefficient of excess reagent (–)
ρ_i	Density of component *i* (g mL^{-1})
τ_{cryst}	Crystalliser residence time (min)

τ_j Residence time in PFR *j* (min)
τ Plant lifetime (y)

7. References

Adamo, A. et al., 2016, On-Demand Continuous-Flow Production of Pharmaceuticals in a Compact, Reconfigurable System, *Science*, 352(6281), 61–67.

Aher, N.G. et al., 2009, Synthesis and antifungal activity of 1,2,3-triazole containing fluconazole analogues, *Bioorg. Med. Chem. Lett.*, 19(3), 759–763.

Alvarez, A.J., Singh, A., Myerson, A.S., 2011, Crystallization of cyclosporine in a multistage continuous MSMPR crystallizer. *Cryst. Growth Des.*, 11(10), 4392–4400.

Ashe, R., 2012, From Batch to Continuous Processing, *Chem. Eng.*, 119(10), 34–40.

Badgujar, D.M. et al., 2008, Advances in science and technology of modern energetic materials: An overview, *J. Haz. Mat.*, 151(2–3), 289–305.

Baumann, M., Baxendale, I.R., Ley, S. V., 2011, The flow synthesis of heterocycles for natural product and medicinal chemistry applications, *Mol. Divers.*, 15(3), 613–630.

Bédard, A.C. et al., 2016, Minimizing E-factor in the continuous-flow synthesis of diazepam and atropine, *Bioorg. Med. Chem.*, 25(23), 6233–6241.

Behr, A. et al., 2004, New Developments in Chemical Engineering for the Production of Drug Substances, *Eng. Life Sci.*, 4, 15–24.

Bonacorso, H.G. et al., 2015, New solventless and metal-free synthesis of the antiepileptic drug 1-(2,6-difluorobenzyl)-1H-1,2,3-triazole-4-carboxamide (Rufinamide) and analogues, *Tetrahedron Lett.*, 56(2), 441–444.

Borukhova, S. et al., 2016, From alcohol to 1,2,3-triazole via a multi-step continuous-flow synthesis of a rufinamide precursor, *Green Chem.*, 99, 9–13.

Borukhova, S. et al., 2013, Solvent- and catalyst-free huisgen cycloaddition to rufinamide in flow with a greener, less expensive dipolarophile, *ChemSusChem*, 6(12), 2220–2225.

Bouillot, B., Teychene, S., Biscans, B., 2011, An Evaluation of Thermodynamic Models for the Prediction of Drug and Drug-like Molecule Solubility in Organic Solvents, *Fluid Phase Equilib.*, 309, 36–52.

Britton, J. et al., 2017, Multi-step continuous-flow synthesis, *Chem. Soc. Rev.*, 52(5), 10159–10162.

Cervera-Padrell, A.E. et al., 2012, Active pharmaceutical ingredient (API) production involving continuous processes - a process system engineering (PSE)-assisted design framework, *Eur. J. Pharm. Biopharm.*, 82(2), 437–56.

Cole-Parmer, 2015, Cole Parmer Polystat Advanced 15L Heat Cool Bath 35 to 200C 115VAC from Cole-Parmer United Kingdom.
http://www.coleparmer.co.uk/Product/Cole_Parmer_Polystat_Advanced_15L_Heat_Cool_Bath_35_to_200C_115VAC/WZ-12122-56.

Corning, 2015. Corning Advanced-Flow G1 SiC Reactor.
http://www.corning.com/media/worldwide/global/documents/G1_SiC_leaflet_FINAL_6.1.15.pdf.

Costa, M.S. et al., 2006, Synthesis, tuberculosis inhibitory activity, and SAR study of N-substituted-phenyl-1,2,3-triazole derivatives, *Bioorg. Med. Chem.*, 14(24), 8644–8653.

Couper, J.R., 2003, *Process Engineering Economics* 1st ed., CRC Press.

Dallinger, D., Kappe, C.O., 2017, Why flow means green – Evaluating the merits of continuous processing in the context of sustainability. *Current Opinion in Green and Sustainable Chemistry*, 7, 6–12.

Diab, S., Gerogiorgis, D.I., 2017a, Process Modeling, Simulation, and Technoeconomic Evaluation of Separation Solvents for the Continuous Pharmaceutical Manufacturing (CPM) of Diphenhydramine, *Org. Process Res. Dev.*, 21(7), 924–946.

Diab, S., Gerogiorgis, D.I., 2017b, Technoeconomic Evaluation of Multiple Mixed Suspension-Mixed Product Removal (MSMPR) Crystallizer Configurations for Continuous Cyclosporine Crystallization, *Org. Process Res. Dev.*, 21(10), 1571–1587.

Federsel, H.-J., 2013, En Route to Full Implementation: Driving the Green Chemistry Agenda in the Pharmaceutical Industry, *Green Chem.*, 15(11), 3105–3115.

Food and Drug Admnistration, 2006. *Review of Environmental Assessment for Inovelon Oral Tablets,*

100, 200 & 400 mg, Ridgefield Park, NJ.
Gutmann, B., Cantillo, D., Kappe, C.O., 2015, Continuous-Flow Technology: A Tool for the Safe Manufacturing of Active Pharmaceutical Ingredients, *Angew. Chem. Int. Ed.*, 54(23), 6688–6728.
Hakimian, S. et al., 2007, Rufinamide: a new anti-epileptic medication, *Expert Opin. Pharmaco.*, 8(12), 1931–1940.
Jimenez-Gonzalez, C. et al., 2011, Using the right green yardstick: Why process mass intensity is used in the pharmaceutical industry to drive more sustainable processes, *Org. Process Res. Dev.*, 15(4), 912–917.
Jolliffe, H.G., Gerogiorgis, D.I., 2016a, Process Modelling and Simulation for Continuous Pharmaceutical Manufacturing of Artemisinin, *Chem. Eng. Res. Des.*, 112, 310–325.
Jolliffe, H.G., Gerogiorgis, D.I., 2016b, Plantwide Design and Economic Evaluation of Two Continuous Pharmaceutical Manufacturing (CPM) Cases: Ibuprofen and Artemisinin, *Comput. Chem. Eng.*, 91(1), 269–288.
Jolliffe, H.G., Gerogiorgis, D.I., 2017a, Technoeconomic optimisation and comparative environmental impact evaluation of continuous crystallisation and antisolvent selection for artemisinin recovery, *Comput. Chem. Eng.*, 103, 218–232.
Jolliffe, H.G., Gerogiorgis, D.I., 2017b, Technoeconomic Optimization of a Conceptual Flowsheet for Continuous Separation of an Analgaesic Active Pharmaceutical Ingredient (API), *Ind. Eng. Chem. Res.*, 56(15), 4357–4376.
Kamal, A. et al., 2008, Synthesis of 1,2,3-triazole-linked pyrrolobenzodiazepine conjugates employing “click” chemistry: DNA-binding affinity and anticancer activity, *Bioorg. Med. Chem. Lett.*, 18(4), 1468–1473.
Kopetzki, D., Levesque, F., Seeberger, P.H., 2013, A Continuous-Flow Process for the Synthesis of Artemisinin, *Chem. Eur. J.*, 19(17), 5450–5456.
Kwon, J.S.-I. et al., 2015, A method for handling batch-to-batch parametric drift using moving horizon estimation: Application to run-to-run MPC of batch crystallization, *Chem. Eng. Sci.*, 127, 210–219.
Li, J. et al., 2017, Continuous Crystallization of Cyclosporine: the Effect of Operating Conditions on Yield and Purity, *Cryst. Growth Des.*, 17(3), 1000–1007.
Mascia, S. et al., 2013, End-to-end Continuous Manufacturing of Pharmaceuticals: Integrated Synthesis, Purification, and Final Dosage Formation, *Angew. Chem. Int. Ed.*, 52(47), 12359–12363.
Miller, M.M. et al., 1985, Relationships between octanol-water partition coefficient and aqueous solubility, *Environm. Sci. Technol.*, 19(6), 522–529.
Mitchell, N.A., Ó’Ciardhá, C.T., Frawley, P.J., 2011, Estimation of the growth kinetics for the cooling crystallisation of paracetamol and ethanol solutions, *J. Cryst. Growth*, 328(1), 39–49.
Morris, G. et al., 2015, Estimation of Nucleation and Growth Kinetics of Benzoic Acid by Population Balance Modeling of a Continuous Cooling Mixed Suspension, Mixed Product Removal Crystallizer, *Org. Process Res. Dev.*, 19(12), 1891–1902.
Movsisyan, M. et al., 2016, Taming hazardous chemistry by continuous flow technology. *Chem. Soc. Rev.*, 45(18), 4892–4928.
Mudd, W.H., Stevens, E.P., 2010, An efficient synthesis of rufinamide, an antiepileptic drug. *Tetrahedron Lett*, 51(24), 3229–3231.
Nagy, Z.K. et al., 2013, Recent advances in the monitoring, modelling and control of crystallization systems, *Chem. Eng. Res. Des.*, 91(10), 1903–1922.
Ott, D., Borukhova, S., Hessel, V., 2016, Life cycle assessment of multi-step rufinamide synthesis – from isolated reactions in batch to continuous microreactor networks, *Green Chem.*, 18(4), 1096–1116.
Plumb, K., 2005, Continuous Processing in the Pharmaceutical Industry - Changing the Mind Set, *Chem. Eng. Res. Des.*, 83(A6), 730–738.
Poechlauer, P. et al., 2013, Pharmaceutical Roundtable Study Demonstrates the Value of Continuous Manufacturing in the Design of Greener Processes, *Org. Process Res. Dev.*, 17(12), 1472–1478.
Power, G. et al., 2015, Design and optimization of a multistage continuous cooling mixed suspension, mixed product removal crystallizer, *Chem. Eng. Sci.*, 133, 125–139.

ProMinent, 2015. Solenoid Driven Metering Pumps.
https://www.prominent.co.uk/en/Products/Products/Metering-Pumps/Solenoid-Driven-Metering-Pumps/pg-solenoid-driven-metering-pumps.html.
Ritter, S.K., 2013, Reducing Environmental Impact of Organic Synthesis, *Chem. Eng. News*, 91(15), 22–23.
Roberge, D.M. et al., 2005, Microreactor technology: A revolution for the fine chemical and pharmaceutical industries?, *Chem. Eng. Technol.*, 28(3), 318–323.
Rogers, A., Ierapetritou, M., 2014, Challenges and Opportunities in Pharmaceutical Manufacturing Modelling and Optimization, *Comput. Aid. Chem. Eng.*, 34, 144–149.
Sang-Il Kwon, J. et al., 2014., Crystal shape and size control using a plug flow crystallization configuration, *Chem. Eng. Sci.*, 119, 30–39.
Schaber, S.D. et al., 2011, Economic Analysis of Integrated Continuous and Batch Pharmaceutical Manufacturing: A Case Study, *Ind. Eng. Chem. Res.*, 50(17), 10083–10092.
Sheldon, R.A., 2012, Fundamentals of Green Chemistry: Efficiency in Reaction Design. *Chem. Soc. Rev.*, 41(4), 1437–1451.
da Silva, F. de C. et al., 2009, Synthesis, HIV-RT inhibitory activity and SAR of 1-benzyl-1H-1,2,3-triazole derivatives of carbohydrates, *Eur. J. Med. Chem.*, 44, 373–383.
Su, Q. et al., 2015. Mathematical Modeling, Design, and Optimization of a Multisegment Multiaddition Plug-Flow Crystallizer for Antisolvent Crystallizations, *Org. Process Res. Dev.*, 19(12), 1859–1870.
Su, Q., Chiu, M.-S. & Braatz, R.D., 2017, Integrated B2B-NMPC control strategy for batch/semibatch crystallization processes, *AIChE J.*, 63(11), 5007–5018.
Teoh, S.K., Rathi, C., Sharratt, P., 2015, Practical Assessment Methodology for Converting Fine Chemicals Processes from Batch to Continuous, *Org. Process Res. Dev.*, 20(2), 414–431.
Wang, X.-L., Wan, K., Zhou, C.-H., 2010, Synthesis of novel sulfanilamide-derived 1,2,3-triazoles and their evaluation for antibacterial and antifungal activities, *Eur. J. Med. Chem.*, 45(10), 4631–4639.
Wilms, D. et al., 2009, Ionic Liquids on Demand in Continuous Flow, *Org. Process Res. Dev.*, 13(5), 961–964.
Woods, D.R., 2007, *Rules of Thumb in Engineering Practice*, 1st ed., Wiley.
Zhang, P., Russell, M.G., Jamison, T.F., 2014, Continuous Flow Total Synthesis of Rufinamide, *Org. Process Res. Dev.*, 18(11), 1567–1570.